
Supervised Quadratic Feature Analysis: An Information Geometry Approach to Dimensionality Reduction

Daniel Herrera-Esposito¹ Johannes Burge¹

Abstract

Supervised dimensionality reduction aims to map labeled data to a low-dimensional feature space while maximizing class discriminability. Despite the availability of methods for learning complex non-linear features (e.g. Deep Learning), there is an enduring demand for dimensionality reduction methods that learn linear features due to their interpretability, low computational cost, and broad applicability. However, there is a gap between methods that optimize linear separability (e.g. LDA), and more flexible but computationally expensive methods that optimize over arbitrary class boundaries (e.g. metric-learning methods). Here, we present Supervised Quadratic Feature Analysis (SQFA), a dimensionality reduction method for learning linear features that maximize the differences between class-conditional first- and second-order statistics, which allow for quadratic discrimination. SQFA exploits the information geometry of second-order statistics in the symmetric positive definite manifold. We show that SQFA features support quadratic discriminability in real-world problems. We also provide a theoretical link, based on information geometry, between SQFA and the Quadratic Discriminant Analysis (QDA) classifier.

1. Introduction

Consider a labeled random variable $\mathbf{x} \in \mathbb{R}^n$ with label $y \in \{1, \dots, c\}$, where c is the number of classes. The goal of supervised dimensionality reduction is to learn a mapping from the variable \mathbf{x} to a lower dimensional variable $\mathbf{z} \in \mathbb{R}^m$ that best supports classification performance. Some modern methods for dimensionality reduction learn non-linear features that lead to good class separation, like deep neural networks (LeCun et al., 2015), manifold learning (Sainburg et al., 2021), and kernel methods (Mika et al.,

1999). These methods, however, require large volumes of data, and their features are often difficult to interpret.

Supervised dimensionality reduction methods that learn linear features are better understood theoretically, and often support good performance, making them a popular choice for many applications (Cunningham & Ghahramani, 2015). The canonical method of this type is Linear Discriminant Analysis (LDA), which aims to optimize the performance of a linear classifier by learning the linear features that maximize the separation between class-conditional means, $\mathbb{E}[\mathbf{z}|y = i]$. (The term ‘LDA’ is usually used to refer to both the dimensionality reduction method and to the classifier. Here, we refer to the former as ‘drLDA’ and to the latter as ‘cLDA’.) Other methods learn linear features that maximize class separability across complex boundaries, like metric-learning methods such as Neighbourhood Components Analysis (Goldberger et al., 2004) and Large Margin Nearest Neighbors (Weinberger & Saul, 2009), but these methods are computationally expensive and often lead to features and class boundaries that are difficult to interpret.

A promising middle-ground is to learn linear features that support discriminability by leveraging the class-conditional first- and second-order statistics of the projected data. Differences in second-order statistics can be used to define quadratic classifiers like the Quadratic Discriminant Analysis (QDA) classifier. Notably, while cLDA and QDA are closely related textbook classification methods, cLDA has a well established dimensionality reduction method counterpart, while QDA does not.

Here, we present Supervised Quadratic Feature Analysis (SQFA), a dimensionality reduction method for learning a set of linear features that support quadratic discriminability. To accomplish this aim, SQFA exploits a relation between class discriminability and the information geometry of symmetric positive definite (SPD) matrices, which represents a novel application of information geometry to machine learning. SQFA balances flexibility, interpretability, and computational simplicity, making it a potentially useful addition to the standard dimensionality reduction toolbox.

¹Department of Psychology, University of Pennsylvania, Pennsylvania, USA. Correspondence to: Daniel Herrera-Esposito <dherrera1911@gmail.com>.

2. Model

2.1. Class statistics notation

The class-conditional second-moment matrices of the variable \mathbf{x} are given by $\Phi_i = \mathbb{E}[\mathbf{x}\mathbf{x}^T|y=i]$. The low-dimensional projection of \mathbf{x} is given by $\mathbf{z} = \mathbf{F}^T \mathbf{x}$, where $\mathbf{F} \in \mathbb{R}^{n \times m}$ is a matrix of filters, and the respective class-conditional means, second moments, and covariances are given by $\mu_i = \mathbb{E}[\mathbf{z}|y=i]$, $\Psi_i = \mathbb{E}[\mathbf{z}\mathbf{z}^T|y=i]$, and $\Sigma_i = \Psi_i - \mu_i \mu_i^T$.

2.2. Geometric loss in the SPD manifold

Our goal is to find linear filters \mathbf{F} such that the class-conditional second-order statistics in the feature space maximize quadratic discriminability (i.e. the ability to separate classes using a quadratic classifier). We first introduce a simpler model making use only of the class-conditional second-moment matrices (i.e. Ψ_i), which we denote smSQFA, and then present in Section 2.4 the model for making use of both class-conditional means and covariances (i.e. μ_i and Σ_i), which we denote SQFA.

Matrices Ψ_i can be considered as points in the manifold of m -by- m SPD matrices, denoted SPD(m) (Figure 1) (Thanwerdas & Pennec, 2023). In SPD(m), Riemannian distances $d(\Psi_i, \Psi_j)$ can be measured between second-moment (or covariance) matrices. The intuition behind our method is that a larger $d(\Psi_i, \Psi_j)$ indicates that the second-moments are more different, and hence, that distance in the manifold should be a good proxy for discriminability of classes i, j (Figure 1). The objective function is then the sum of pairwise distances

$$\arg \max_{\mathbf{F} \in \mathbb{R}^{n \times m}} \frac{1}{2} \sum_{i=1}^c \sum_{j=1}^c d_{AI}(\Psi_i, \Psi_j) \quad (1)$$

where d_{AI} is the affine-invariant distance and the factor of $1/2$ accounts for double counting of class pairs. This objective should be a good proxy for the simultaneous discriminability of all class pairs.

2.3. Affine-invariant distance and discriminability

Many Riemannian distances are compatible with the SPD(m) manifold. The affine-invariant distance is the most commonly used. It is given by

$$\begin{aligned} d_{AI}(\Psi_i, \Psi_j) &= \left\| \log(\Psi_i^{-1/2} \Psi_j \Psi_i^{-1/2}) \right\|_F \\ &= \sqrt{\sum_{k=1}^m \log^2 \lambda_k}. \end{aligned} \quad (2)$$

where \log is the matrix logarithm, $\|\cdot\|_F$ is the Frobenius norm, and λ_k is the k -th generalized eigenvalue of the pair

of matrices (Ψ_i, Ψ_j) . Some properties of d_{AI} make it a sensible proxy for quadratic discriminability.

2.3.1. d_{AI} SUMMARIZES QUADRATIC DIFFERENCES

For classes i, j , the squared norm of the projection of \mathbf{z} onto the k -th generalized eigenvector of (Ψ_i, Ψ_j) , \mathbf{v}_k , satisfies

$$\lambda_k = \frac{\mathbb{E}[(\mathbf{v}_k^T \mathbf{z})^2 | y=i]}{\mathbb{E}[(\mathbf{v}_k^T \mathbf{z})^2 | y=j]} \quad (3)$$

(see Appendix A.1). The more different λ_k is from 1, the more different the squared projections of \mathbf{z} will be along the direction of \mathbf{v}_k for classes i, j . The magnitude of $\log^2 \lambda_k$ indicates how different the ratio in Equation (3) is from 1, in proportional terms. Because the set of \mathbf{v}_k 's spans the space of \mathbf{z} , d_{AI} summarizes the squared differences between classes the i, j in the feature space (see Equation (2)), and so should reflect the quadratic discriminability of the classes in this space.

2.3.2. d_{AI} IS INDUCED BY THE FISHER INFORMATION METRIC

The affine-invariant distance is induced by the Fisher information metric for zero-mean Gaussian distributions (Atkinson & Mitchell, 1981), which is a local measure of discriminability (see Appendix A.2 for an explanation of metrics). Therefore, it is the same as the information-geometric distance between zero-mean Gaussians (Amari, 2016).

Fisher information measures how well distribution $p(\mathbf{z}|\theta)$, defined by parameter vector θ , can be discriminated from a neighboring distribution obtained by perturbing θ in the direction of θ' . Denoting $l(\mathbf{z}) = \log p(\mathbf{z}|\theta)$, the gradient $\nabla_{\theta} l(\mathbf{z})$ with respect to θ is called the score function. The Fisher information of $p(\mathbf{z}|\theta)$ along direction θ' of a perturbation is defined as $\mathcal{I}_{\theta}(\theta') = \mathbb{E}[(\nabla_{\theta} l(\mathbf{z}) \cdot \theta')^2]$, where the expectation is taken over \mathbf{z} . The quantity $\sqrt{\mathcal{I}_{\theta}(\theta')}$ is a measure of how discriminable $p(\mathbf{z}|\theta)$ is from $p(\mathbf{z}|\theta + \epsilon\theta')$, where $\epsilon\theta'$ is the infinitesimal perturbation in direction θ' . This quantity is often used in statistical signal processing and in neuroscience to measure the local discriminability of a signal θ given a stochastic observation or neural response \mathbf{z} (Ly et al., 2017; Ding et al., 2023; Feather et al., 2024; Ni & Burge, 2024).

Let the curve $\Psi(t)$ in SPD(m) be the affine-invariant geodesic from Ψ_i to Ψ_j , with $\Psi(0) = \Psi_i$, $\Psi(1) = \Psi_j$, and velocity $\Psi'(t)$ at point $\Psi(t)$. Consider the set of zero-centered Gaussian distributions $p(\mathbf{z}|\Psi(t)) = \mathcal{N}(0, \Psi(t))$ for each $\Psi(t)$ along the geodesic. The Fisher information of $p(\mathbf{z}|\Psi(t))$ in the direction of the geodesic is

$$\mathcal{I}_{\Psi(t)}(\Psi'(t)) = \frac{1}{2} \text{Tr}(\Psi^{-1}(t) \Psi'(t) \Psi^{-1}(t) \Psi'(t)) \quad (4)$$

and $\sqrt{\mathcal{I}_{\Psi(t)}(\Psi'(t))}$ is a measure of how discriminable

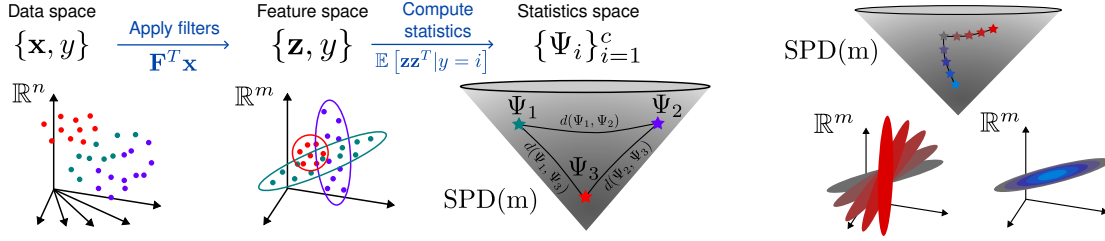


Figure 1. SQFA uses a geometric proxy of discriminability. **Left.** SQFA maps the n -dimensional data into an m -dimensional feature space using the linear filters \mathbf{F} . The class-specific statistics in the feature space are represented as points in the $\text{SPD}(m)$ manifold (which is an open cone). The distances in $\text{SPD}(m)$ are a proxy for discriminability. **Right.** Each point in $\text{SPD}(m)$ (top) corresponds to a second-moment ellipse (below). As the distance in $\text{SPD}(m)$ increases, the second-order statistics become more different.

$\mathcal{N}(0, \Psi(t))$ is from $\mathcal{N}(0, \Psi(t + dt))$. Equation (4) is equal to $\|\Psi'(t)\|^2$ (up to a factor of 2), under the affine-invariant metric (Atkinson & Mitchell, 1981). Integrating the speed (i.e. norm of the velocity) of the geodesic to obtain its length, and denoting $\mathcal{I}(t) = \mathcal{I}_{\Psi(t)}(\Psi'(t))$, we obtain

$$d_{AI}(\Psi_i, \Psi_j) = \int_0^1 \sqrt{2\mathcal{I}(t)} dt \quad (5)$$

So, $d_{AI}(\Psi_i, \Psi_j)$ can be conceptualized as the accumulated discriminability of the infinitesimal perturbations transforming $\mathcal{N}(0, \Psi_i)$ into $\mathcal{N}(0, \Psi_j)$ along the geodesic, suggesting that d_{AI} is a sensible proxy for quadratic discriminability¹.

In addition to these theoretical considerations, we show in Appendix A.3 that other distances in $\text{SPD}(m)$ (e.g. Wasserstein distance) learn less discriminative features than d_{AI} .

2.4. Fisher-Rao distances for class means and covariances

The model described thus far, denoted smSQFA, uses class-conditional second-moment matrices only. It is more informative to make use of both the class-conditional means and second-moment matrices (or covariances). To do so, we consider each class as a point in the manifold of Gaussian distributions. In this manifold, the Fisher-Rao distance again provides a proxy for quadratic discriminability (via similar reasoning as with zero-centered Gaussians; see Section 2.3.2). We refer to this more general method as SQFA.

Unfortunately, there is no closed-form expression for the Fisher-Rao distance in this space (Miyamoto et al., 2024). However, a lower bound to the Fisher-Rao distance can be obtained by embedding the statistics (μ_i, Σ_i) into

¹Note that although there is a formal link between d_{AI} and local discriminability, this reasoning does not formally link d_{AI} to a quantitative measure of discriminability between far away (i.e. non-infinitesimally close) distributions.

$\text{SPD}(m+1)$ as follows

$$\Omega_i = \begin{bmatrix} \Sigma_i + \mu_i \mu_i^T & \mu_i \\ \mu_i^T & 1 \end{bmatrix} \quad (6)$$

The Fisher-Rao distance between two distributions $\mathcal{N}(\mu_i, \Sigma_i)$ and $\mathcal{N}(\mu_j, \Sigma_j)$ is bounded from below by the distance $d_{AI}(\Omega_i, \Omega_j)$ in $\text{SPD}(m+1)$ (Calvo & Oller, 1990). Thus, to consider class means and covariances separately, one can embed the class-specific means and covariances into $\text{SPD}(m+1)$, and maximize the affine-invariant distances between classes just as before. Better approximations of the Fisher-Rao distance exist, but they require more complex implementations and are more computationally expensive (Nielsen, 2023). Future work should explore whether these better approximations improve SQFA performance.

2.5. LDA is a special case of SQFA

The previous section described the most general case of SQFA. Here, we show that under certain conditions SQFA reduces to LDA. Specifically, when $\Sigma_i = \Sigma$ for all i , the Fisher-Rao distance between classes i, j , denoted $d_{\Sigma}(\mu_i, \mu_j)$, has a closed-form expression given by the Mahalanobis distance (Pinele et al., 2020). In this case, the following proposition holds.

Proposition 2.1. *If $\Sigma_i = \Sigma$ for all classes i , then*

$$\frac{1}{2} \sum_{i=1}^c \sum_{j=1}^c d_{\Sigma}(\mu_i, \mu_j)^2 = c \text{Tr}(\Sigma^{-1} \mathbf{S}_B) \quad (7)$$

where $\mu = \frac{1}{c} \sum_{i=1}^c \mu_i$ and $\mathbf{S}_B = \frac{1}{c} \sum_{i=1}^c (\mu_i - \mu)(\mu_i - \mu)^T$ is the between-class scatter matrix.

For a proof, see Appendix C.

The right-hand side of Equation (7) is the objective function of drLDA times a constant. Thus, the objective of drLDA is the same as the objective of SQFA when the class-conditional covariances are equal².

²SQFA uses distances rather than squared distances, because

From the perspective of information geometry, SQFA is to QDA what drLDA is to cLDA. Both dimensionality reduction methods maximize the Fisher-Rao distances between classes under the distributional assumptions of the respective classifiers. Thus, drLDA is a special case of SQFA in the same way that cLDA is a special case of QDA.

2.6. Learning

2.6.1. OPTIMIZATION

Filters \mathbf{F} are initialized to the first m PCA components of the dataset, and then learned by optimizing Equation (1) with the L-BFGS gradient descent algorithm until convergence. We add a small constant inside the square root in Equation (2) for numerical stability. Filters are constrained to have unit norm.

We note that to compute the class statistics on each iteration, only the data statistics are needed, and not the raw data itself, so SQFA only needs access to the data statistics.

2.6.2. REGULARIZATION

In real world applications, the second-moment matrices of the raw data can be rank-deficient. Under such circumstances, SQFA can obtain rank-deficient second-moment matrices, resulting in infinite pairwise distances. This can be prevented by adding a regularization term: $\Psi_i = \mathbf{F}^T \Phi_i \mathbf{F} + \mathbf{I}_m \sigma^2$, where \mathbf{I}_m is the identity matrix and σ^2 is a regularization parameter and Φ_i is the second-moment matrix of the raw data for class i . Regularization makes training more stable, but it can mask relevant information in low-variance subspaces. σ^2 was set manually for each dataset to maximize performance. Future work should explore ways to set σ^2 automatically, or alternative regularization methods such as covariance shrinkage (Ledoit & Wolf, 2022).

2.6.3. INVARIANCE AND UNIQUENESS

The affine-invariant distance is invariant to invertible linear transformations of the feature vector. In the absence of regularization (that is, $\sigma^2 = 0$), this implies that the solution to Equation (1) is only unique up to an invertible linear combination of the filters. However, when regularization is used, the equivalence of solutions is broken (see Appendix B)

Also, the ordering of the filters is not unique. In some applications, it may be desirable for the filters to be ordered by usefulness. Such ordering can, for example, be achieved by learning the filters in pairs. If two filters are learned first, then this pair can be fixed and two more can be learned, and so on, until the desired number of filters is reached.

these were found to lead to higher QDA accuracies in the tested datasets (see Section 2.7). Strictly speaking, drLDA is a special case of a variant of SQFA that uses squared distances.

The first pair will be the most discriminative pair, the next pair will be the next most discriminative pair (when used in conjunction with the first pair), and so on. (Filters could also be learned one at a time, or in triplets, etc.) A downside of this approach is that the set of sequentially learned filters might not be as discriminative as the set of filters learned all at once.

2.7. Comparison to other methods

To compare SQFA and smSQFA to other linear dimensionality reduction methods, we learned a set of features with each method, and then computed the accuracy of the QDA classifier trained using the features learned by each method. We compared SQFA and smSQFA to PCA, drLDA, Independent Component Analysis (ICA), Factor Analysis (FA), and to the metric-learning method Large Margin Nearest Neighbors (LMNN) (Weinberger & Saul, 2009)³. We used scikit-learn for PCA, drLDA, ICA, FA, and the QDA classifier (Pedregosa et al., 2011), and the metric-learn library for LMNN (Vazelhes et al., 2020). We used default parameters, except for drLDA, where we manually set the regularization parameter to maximize QDA accuracy.

A Python package implementing SQFA is available at <https://github.com/dherrera1911/sqfa>.

3. Related work

Because SQFA is a dimensionality reduction method for finding linear features, in this section we describe other well-known methods for finding linear features. There are a large number of such methods that cannot be covered here; for a review see (Cunningham & Ghahramani, 2015).

3.1. Unsupervised dimensionality reduction

Unsupervised dimensionality reduction methods do not use class labels, and typically aim to preserve the variance of the data or to find features with statistical properties like independence or sparsity. The most popular method of this kind is PCA, which finds the orthonormal linear filters \mathbf{F} that maximize the variance of the projected data $\mathbf{z} = \mathbf{F}^T \mathbf{x}$.

Although unsupervised methods do not use class labels, some assume that an unobserved low-dimensional latent variable generates the observed raw data. For example, FA assumes that the data is generated by a linear transformation of a low-dimensional latent variable \mathbf{z} plus Gaussian noise, $\mathbf{x} = \mathbf{A}\mathbf{z} + \eta$, where $\mathbf{A} \in \mathbb{R}^{n \times m}$ is a matrix of factor loadings and $\eta \sim \mathcal{N}(0, \mathbf{D})$ is Gaussian noise with diagonal

³For LMNN we also projected the dataset to the first 100 principal components and downsampled by 10 the number of training samples, due to its high computational cost. The results of the other methods changed only slightly when using the reduced datasets.

covariance \mathbf{D} . FA learns the loadings \mathbf{A} and covariance \mathbf{D} that maximize the likelihood of the data. Another example is ICA. It assumes that \mathbf{x} is generated by a linear transformation $\mathbf{x} = \mathbf{A}\mathbf{z}$, where $\mathbf{A} \in \mathbb{R}^{n \times m}$ is a mixing matrix and \mathbf{z} is the (low-dimensional) source variable. ICA aims to learn the filters \mathbf{F} (i.e. the pseudo-inverse of \mathbf{A}) that maximize the independence of the sources $\mathbf{z} = \mathbf{F}^T \mathbf{x}$.

SQFA has a fundamentally different goal than these methods in that it is supervised, so it uses class labels to maximize discriminability. One possible source of confusion is that the class label y is, in some literatures (e.g. neuroscience), often referred to as a latent variable, which might suggest to some readers that FA and ICA exploit the same class information as SQFA. However, as suggested by our notation, the latent variable in FA and ICA is more akin to the feature vector \mathbf{z} in SQFA, which is not class specific.

3.2. Supervised dimensionality reduction

The most popular supervised linear dimensionality reduction method is drLDA, which aims to learn the features that maximize linear separability between classes. This is accomplished by maximizing the ratio of the between-class variance to the within-class variance in the projected data $\mathbf{z} = \mathbf{F}^T \mathbf{x}$. Unlike SQFA, drLDA does not use class-conditional second moments (or covariances). Instead, it assumes a common within-class covariance matrix. The features learned by drLDA maximize the performance of the cLDA classifier, which has linear classification boundaries because it assumes Gaussian class-conditional distributions and identical within-class covariances (homoscedasticity). The advantage of SQFA over drLDA is that the former can learn features that also support quadratic discriminability.

Within linear dimensionality reduction methods, there is one relevant example that aims to maximize quadratic discriminability, which we refer to as the Generalized Eigenvector Method (GEM) (Karampatziakis & Mineiro, 2014). GEM proposes using as features the generalized eigenvectors of pairs of class-specific second-moment matrices of the raw data (Φ_i, Φ_j) . However, one crucial drawback of GEM is that it learns a set of features specific for each pair of classes. The number of features therefore scales quadratically with the number of classes, leading to a potentially high number of features. Additionally, because features are learned for each pair of classes, the features can be, and often will be, redundant. SQFA, on the other hand, learns a single low-dimensional set of features that maximizes second-order differences between all classes simultaneously.

Other methods learn features that optimize for more complex criteria of class separation, which can be exploited by classifiers like k-Nearest Neighbors (kNN). Wasserstein Discriminant Analysis (WDA), for example, maximizes the regularized Wasserstein distance between the class-conditional

empirical distributions. As does SQFA, WDA takes an information geometric approach. (Interestingly, like for SQFA, drLDA is a special case of WDA.) (Flamary et al., 2018). Another popular class of state-of-the-art techniques are metric-learning methods (e.g. LMNN (Weinberger & Saul, 2009)), which learn linear features that push within-class samples closer together and between-class samples farther apart. These methods typically aim to maximize the performance of kNN classifiers.

Although WDA and LMNN can learn features with more complex class separability than SQFA, the latter has important advantages. First, the computational cost of SQFA is considerably lower, and its cost does not scale with the number of data points (see Appendix D). Second, SQFA operates only on the class-conditional data statistics, and not on the raw data itself. This can be a substantial benefit for some applications (see Discussion). Third, quadratic classifiers can be more interpretable than kNN classifiers, especially when the data is modeled as Gaussian class-conditional distributions, as assumed by QDA.

3.3. Methods maximizing distances in manifolds

Geometry-aware PCA (gaPCA) also deserves a specific mention (Harandi et al., 2014). gaPCA is an unsupervised dimensionality reduction method for data in the SPD manifold. (As an example, gaPCA is typically used for EEG data where each trial can be represented as an SPD matrix (Lotte et al., 2018).) For a set of observations $\{\mathbf{X}_q\}_{q=1}^N$ where $\mathbf{X}_q \in \text{SPD}(n)$, gaPCA learns a set of filters \mathbf{F} to map the dataset to the lower dimensional $\text{SPD}(m)$ manifold using the transformation $\mathbf{Z}_q = \mathbf{F}^T \mathbf{X}_q \mathbf{F}$. The goal of gaPCA is to maximize the variance of the transformed dataset $\{\mathbf{Z}_q\}_{q=1}^N$. Remarkably, the goal of gaPCA—to maximize the variance of the transformed SPD matrices—leads to an optimization problem that is almost identical to that in Equation (1).

However, the different goals of SQFA and gaPCA lead to important differences between the two methods. One difference is that SQFA requires that the loss in Equation (1) be a good proxy for discriminability in the underlying \mathbb{R}^m feature space, while this is not necessary for gaPCA (e.g., which could use a distance which is not a good proxy for discriminability). Another is that, because of its goal of maximizing quadratic discriminability, the embedding in Equation (6) is a useful tool for SQFA, but such an embedding does not make sense for gaPCA.

4. Results

4.1. Toy problem: SQFA vs. drLDA vs. PCA

First, we illustrate the differences between SQFA, drLDA, and PCA, using a toy dataset with three classes and six dimensions. The raw data is designed such that there are

three different two-dimensional subspaces that are each preferred by one of the techniques (Figure 2). Dimensions 1-2 contain very different and discriminable class-specific covariances, so these dimensions are favored by SQFA; because these dimensions contain no differences in means and moderate variance, they are non-preferred by PCA and drLDA. Dimensions 3-4 contain differences in the class-specific means, so they are preferred by drLDA, but these dimensions do not support good discrimination, so they are non-preferred by SQFA. Dimensions 5-6 contain high variance, so they are preferred by PCA, but they do not support discrimination at all. The learned filters show the expected preference of each method, and the SQFA filters select for the most discriminative subspace.

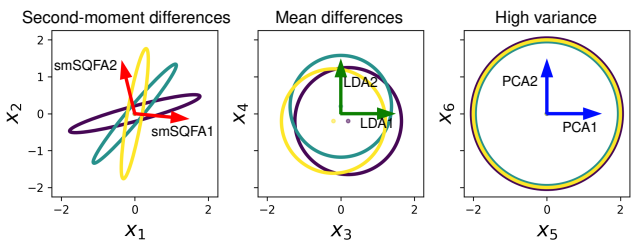


Figure 2. Toy problem 1. Ellipses represent 6D Gaussian-distributed raw data for each of three different classes (colors). Each panel shows two data-dimensions, where the classes are distinguished by different statistical properties (left: covariances; middle: means; right: neither). We learned two filters each with SQFA, drLDA, and PCA (arrows). Each dimensionality reduction technique prefers a different subspace.

Next, we illustrate the differences between SQFA and smSQFA, using a second toy problem with four dimensions, where the dimensions 1-2 and dimensions 3-4 have almost identical second-moment matrices, but very different means and covariances. While in dimensions 1-2 the classes have very different means and the same covariance, in dimensions 3-4 they all have zero mean and different covariances. The second-moment matrices are slightly more different for dimensions 3-4, making them preferred by smSQFA, while dimensions 1-2 are more discriminative, making them preferred by SQFA (Figure 3).

4.2. SQFA for digit classification with poor first-order information

To test whether SQFA can recover linear features useful for quadratic discrimination in a real-world problem, we compared SQFA to other methods using the Street View House Numbers (SVHN) dataset. We expect that first-order differences are not enough to discriminate between the digits in this dataset, because of the many sources of variation in the images (e.g. variation in background intensity, and in the polarity of the digits), so that second-order differences

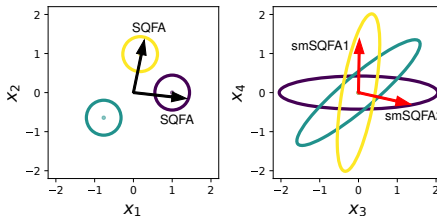


Figure 3. Toy problem 2. Ellipses represent 4D Gaussian-distributed raw data for each of three different classes (colors). The second-moment matrices are almost identical for dimensions 1-2 and 3-4, but they are slightly more different in dimensions 3-4 than in dimensions 1-2. The differences in the means make dimensions 1-2 much more discriminative. SQFA learns features that select for the subspace in which the classes are most discriminable, regardless of whether the useful information is in the means or covariances. smSQFA features select for the subspace most discriminative in terms only of its second-moments.

are necessary for discrimination. We learned nine filters with different methods and tested the accuracy of a QDA classifier using the features learned by each method. (drLDA is limited to the number of classes minus one filters, which in the present case is nine, so the same number of filters were used for all methods for comparison.)

The filters learned by SQFA and smSQFA show a more digit-like structure than those learned by other methods (Figure 4), indicating that they can extract meaningful features from complex data. The similarity between SQFA and smSQFA suggests that, for this dataset, the class means are not very informative. QDA accuracy is higher for the SQFA features than for the features learned with other methods. Thus, SQFA successfully captures features useful for quadratic discrimination. Importantly, the only method to learn features faster than SQFA and smSQFA was PCA (Appendix D), showing that SQFA is computationally efficient.

4.3. SQFA for digit classification with useful first-order information

To test whether SQFA can effectively use both class means and covariances, we next tested the model on MNIST, a dataset where we expect the class means to be informative because of the highly structured data. We again learned nine filters with the different methods (Figure 5).

Accuracy was higher for SQFA features than for all other methods, except LMNN, which had the same accuracy (although SQFA trained 2 orders of magnitude faster, Appendix D). This shows that SQFA makes use of first- and second-order statistics in a way that allows it to outperform drLDA and smSQFA, which use one or the other (Figure 5). Interestingly, drLDA features outperformed smSQFA fea-

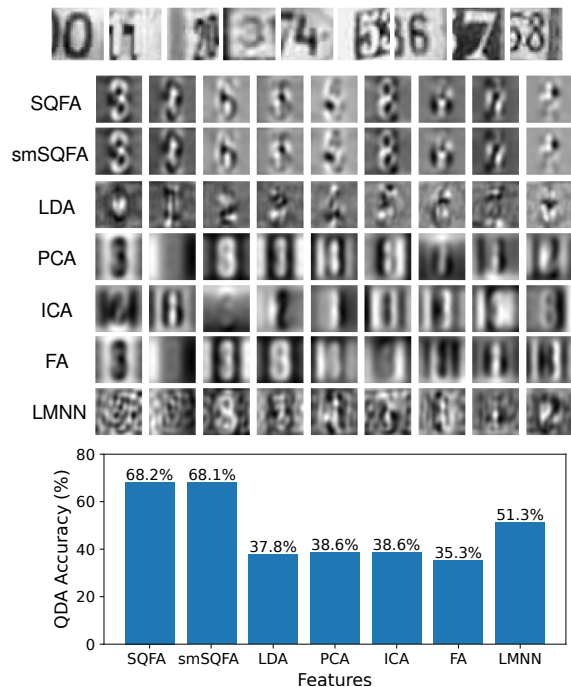


Figure 4. SQFA extracts useful features using class-conditional first- and second-order statistics, outperforming related methods. **Top.** Example images from SVHN. **Center.** Filters learned with different methods. **Bottom.** QDA accuracy using the features learned by the different methods.

tures, showing that the latter can miss relevant information that is present in the class means.

4.4. Naturalistic speed estimation task

How do SQFA features compare to optimal features for quadratic discrimination? To answer this, we tested SQFA with a speed estimation dataset used in previous work in computational neuroscience (Burge & Geisler, 2015; Chin & Burge, 2020). This dataset is interesting for different reasons. First, because the class means approximately equal zero, and most of the task-relevant information is in the covariance structure of the videos, the task is particularly suitable for SQFA. Because the class means carry little task-relevant information, SQFA and smSQFA should perform near-identically. Second, a technique called AMA-Gauss has been used to find features that maximize the performance of a Bayesian decoder analogous to QDA (Jaini & Burge, 2017; Herrera-Esposito & Burge, 2024), providing a useful benchmark. Finally, finding features (receptive fields) that are useful for solving visual tasks is essential for systems neuroscience and perception science (Burge, 2020), which is a potential application area for SQFA.

The videos in the dataset consist of 30 horizontal pixels and

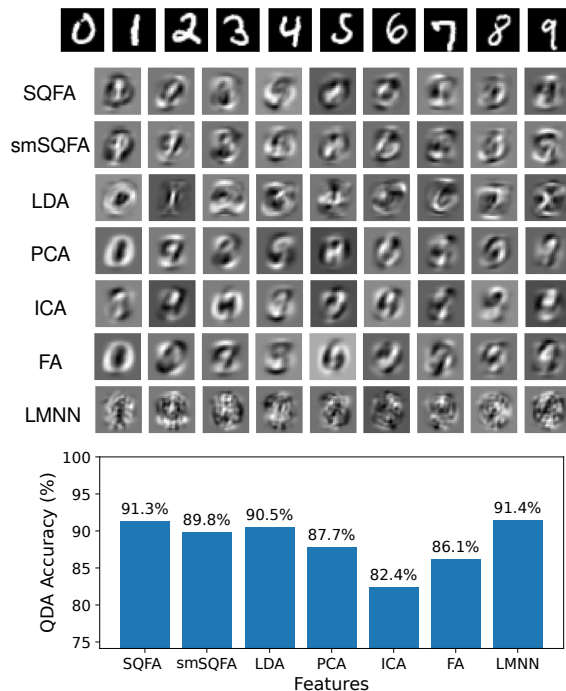


Figure 5. SQFA can exploit class-conditional first- and second-order information. **Top.** Example images from MNIST. **Center.** Filters learned with different methods. **Bottom.** QDA accuracy using the features learned by the different methods.

15 frames. The vertical dimension was averaged out; thus videos can be represented as 2D space-time plots (Figure 6). Each video shows a textured surface moving with one of 41 different speeds (i.e. classes). We learned 8 filters with each method. (See Appendix E for more details on the dataset and AMA-Gauss.) SQFA filters were learned sequentially in pairs to aid interpretability (see Section 2.6.3).

Both SQFA and AMA-Gauss learn filters similar to the typical motion-selective filters found in the visual cortex (Movshon et al., 1978; Rust et al., 2005), covering a range of spatio-temporal frequencies (Figure 6). In contrast, the filters learned by the other methods either lack clear motion-selectivity, or do not cover a range of spatio-temporal frequencies. This result again shows that SQFA can extract interpretable features from complex datasets. QDA accuracy was higher for the SQFA and smSQFA features than for all the other methods except AMA-Gauss, but the difference was relatively small. Thus, SQFA captured close to optimal features for quadratic classification in this task, but there is room for improvement.

Why is SQFA outperformed by AMA-Gauss in this task? One reason might be that the AMA-Gauss method explicitly optimizes the performance of a probabilistic decoder, which is a more direct measure of discriminability than

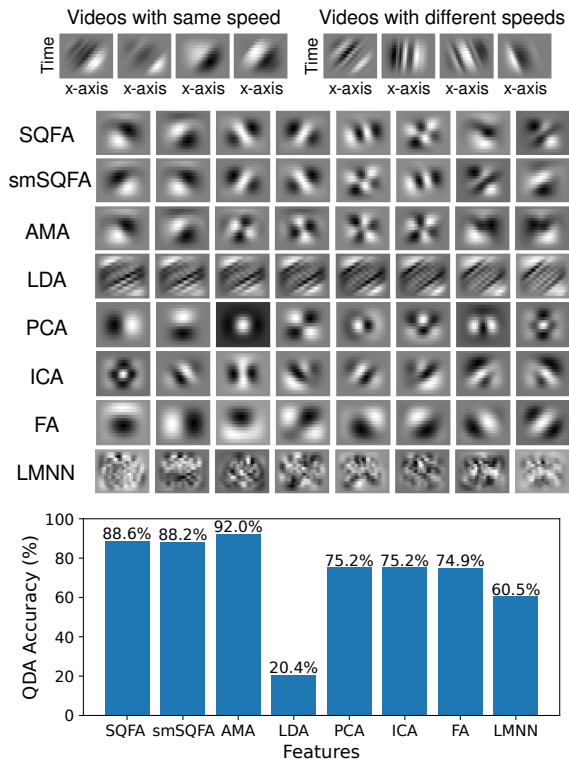


Figure 6. SQFA features are close to optimal for quadratic discrimination. **Top.** 4 example videos with the same speed (left) and 4 example videos with different speeds (right). Each video is shown as a 2D space-time plot where the vertical axis is time and the horizontal axis is space. **Center.** Filters learned different methods (each image shows a 2D space-time plot). **Bottom.** Performance of a QDA classifier using the filters learned by the different methods.

affine-invariant distances. Another reason might be that taking the average of pairwise affine-invariant (or Fisher-Rao) distances between classes might not be a perfect proxy for quadratic discriminability across classes.

5. Discussion

We have introduced SQFA, a supervised dimensionality reduction method for learning linear features that support quadratic classifiers like QDA. SQFA strikes a balance between flexibility and interpretability, at a low computational cost. We showed on three different real-world datasets that SQFA can learn features that support quadratic classification, with a computational cost comparable to standard methods like drLDA. SQFA is based on a novel information geometric approach that maximizes the Fisher-Rao distances between class-conditional statistics.

Notably, we showed that drLDA is a special case of SQFA, and that from an information geometry perspective, SQFA is to QDA what drLDA is to cLDA. QDA is useful in many

applications because it is one of the simplest non-linear classifiers, relying on a class-conditional Gaussian model of the data with nice theoretical properties. However, one of the shortcomings of QDA as compared to cLDA, is that it requires estimating a larger number of parameters, making it more prone to overfitting. SQFA has the potential to make QDA more practical by reducing the dimensionality of the data in a way that is useful for quadratic classification.

A useful feature of SQFA is that it requires only the first- and second-order class-specific statistics of the data. Thus, it can be used when class-conditional statistics are available but the raw data itself is not (e.g. unlike AMA-Gauss or LMNN that operate on the raw data). A possible application of this is in neuroscience, where recent modeling work allows to estimate the covariance structure of neural responses in unobserved experimental conditions (Nejatbakhsh et al., 2023; Ding et al., 2023; Maheswaranathan et al., 2023), and where second-order response statistics are known to be essential to neural coding (Moreno-Bote et al., 2014; Kohn et al., 2016). In this context, SQFA can be used for the identification of the modes of neural population activity that are most useful for decoding by downstream neural circuits, a problem that is of interest in systems neuroscience.

SQFA could also motivate further research at the intersection of information geometry and machine learning. For example, while we provided arguments for the usefulness of Fisher-Rao distances as a proxy for discriminability, and empirically showed its effectiveness, we did not provide a formal link between Fisher-Rao distances and a quantitative measure of discriminability. Such a formal link does not exist in the literature, to our knowledge (although Fisher-Rao distances have been used for supervised learning in other contexts, see (Miyamoto et al., 2023)). SQFA provides a motivation for the study of such a link.

Another topic of interest is the relation of SQFA to other methods that use distances between probability distributions for learning. In this work, we used affine-invariant and Fisher-Rao distances. In supplemental analyses, we found that the Wasserstein distance is not as good a proxy for discriminability. But Wasserstein distances have been successful in many other machine learning applications (Arjovsky et al., 2017; Flamary et al., 2018; Montesuma et al., 2025). A more systematic understanding of the potential advantages and disadvantages of different Riemannian distances for learning is another intriguing direction for future work.

In conclusion, SQFA is a linear dimensionality reduction method that should find broad application in machine learning, statistics, and neuroscience. Its novel information geometric approach motivates several questions about the relationship between Fisher-Rao distances and discriminability that are of practical and theoretical interest.

References

- Amari, S.-i. *Information Geometry and Its Applications*. Springer, February 2016. ISBN 978-4-431-55978-8. Google-Books-ID: UksFCwAAQBAJ.
- Arjovsky, M., Chintala, S., and Bottou, L. Wasserstein Generative Adversarial Networks. In *Proceedings of the 34th International Conference on Machine Learning*, pp. 214–223. PMLR, July 2017. URL <https://proceedings.mlr.press/v70/arjovsky17a.html>. ISSN: 2640-3498.
- Arsigny, V., Fillard, P., Pennec, X., and Ayache, N. Log-Euclidean metrics for fast and simple calculus on diffusion tensors. *Magnetic Resonance in Medicine*, 56(2):411–421, 2006. ISSN 1522-2594. doi: 10.1002/mrm.20965. URL <https://onlinelibrary.wiley.com/doi/abs/10.1002/mrm.20965>. eprint: <https://onlinelibrary.wiley.com/doi/pdf/10.1002/mrm.20965>.
- Atkinson, C. and Mitchell, A. F. S. Rao’s Distance Measure. *Sankhyā: The Indian Journal of Statistics, Series A (1961-2002)*, 43(3):345–365, 1981. ISSN 0581-572X. URL <https://www.jstor.org/stable/25050283>. Publisher: Springer.
- Burge, J. Image-Computable Ideal Observers for Tasks with Natural Stimuli. *Annual Review of Vision Science*, 6(1):491–517, 2020. doi: 10.1146/annurev-vision-030320-041134. URL <https://doi.org/10.1146/annurev-vision-030320-041134>. eprint: <https://doi.org/10.1146/annurev-vision-030320-041134>.
- Burge, J. and Geisler, W. S. Optimal speed estimation in natural image movies predicts human performance. *Nature Communications*, 6(1):7900, August 2015. ISSN 2041-1723. doi: 10.1038/ncomms8900. URL <https://www.nature.com/articles/ncomms8900>. Publisher: Nature Publishing Group.
- Calvo, M. and Oller, J. M. A distance between multivariate normal distributions based in an embedding into the siegel group. *Journal of Multivariate Analysis*, 35(2):223–242, November 1990. ISSN 0047-259X. doi: 10.1016/0047-259X(90)90026-E. URL <https://www.sciencedirect.com/science/article/pii/0047259X9090026E>.
- Chin, B. M. and Burge, J. Predicting the Partition of Behavioral Variability in Speed Perception with Naturalistic Stimuli. *The Journal of Neuroscience*, 40(4):864–879, January 2020. ISSN 0270-6474, 1529-2401. doi: 10.1523/JNEUROSCI.1904-19.2019. URL <https://www.jneurosci.org/lookup/doi/10.1523/JNEUROSCI.1904-19.2019>.
- Congedo, M. and Jain, S. A Julia Package for manipulating Brain-Computer Interface Data in the Manifold of Positive Definite Matrices. In *2019 IEEE International Conference on Systems, Man and Cybernetics (SMC)*, pp. 211–216, Bari, Italy, October 2019. IEEE. ISBN 978-1-72814-569-3. doi: 10.1109/SMC.2019.8914223. URL <https://ieeexplore.ieee.org/document/8914223/>.
- Cunningham, J. P. and Ghahramani, Z. Linear Dimensionality Reduction: Survey, Insights, and Generalizations. *Journal of Machine Learning Research*, 16:2859–2900, 2015.
- Ding, X., Lee, D., Melander, J., Sivulka, G., Ganguli, S., and Baccus, S. Information Geometry of the Retinal Representation Manifold. *Advances in Neural Information Processing Systems*, 36:44310–44322, December 2023. URL https://proceedings.neurips.cc/paper_files/paper/2023/hash/8a267516a7a697965c6ae4f48b908605-Abstract-Conference.html.
- Feather, J., Lipshutz, D., Harvey, S. E., Williams, A. H., and Simoncelli, E. P. Discriminating image representations with principal distortions, October 2024. URL <http://arxiv.org/abs/2410.15433>. arXiv:2410.15433 [q-bio].
- Flamary, R., Cuturi, M., Courty, N., and Rakotomamonjy, A. Wasserstein discriminant analysis. *Machine Learning*, 107(12):1923–1945, December 2018. ISSN 1573-0565. doi: 10.1007/s10994-018-5717-1. URL <https://doi.org/10.1007/s10994-018-5717-1>.
- Goldberger, J., Hinton, G. E., Roweis, S., and Salakhutdinov, R. R. Neighbourhood Components Analysis. In *Advances in Neural Information Processing Systems*, volume 17. MIT Press, 2004. URL <https://proceedings.neurips.cc/paper/2004/hash/42fe880812925e520249e808937738d2-Abstract.html>.
- Guigui, N., Miolane, N., and Pennec, X. Introduction to Riemannian Geometry and Geometric Statistics: From Basic Theory to Implementation with Geomstats. *Foundations and Trends® in Machine Learning*, 16(3):329–493, February 2023. ISSN 1935-8237, 1935-8245. doi: 10.1561/22000000098. URL <https://www.nowpublishers.com/article/Details/MAL-098>. Publisher: Now Publishers, Inc.
- Harandi, M. T., Salzmann, M., and Hartley, R. From Manifold to Manifold: Geometry-aware Dimensionality Reduction for SPD Matrices. In *Computer Vision – ECCV 2014*, volume 8690, pp.

- 17–32, Cham, 2014. Springer International Publishing. ISBN 978-3-319-10604-5 978-3-319-10605-2. doi: https://doi.org/10.1007/978-3-319-10605-2_2. URL http://link.springer.com/10.1007/978-3-319-10605-2_2.
- Herrera-Esposito, D. and Burge, J. Optimal estimation of local motion-in-depth with naturalistic stimuli. *Journal of Neuroscience*, November 2024. ISSN 0270-6474, 1529-2401. doi: 10.1523/JNEUROSCI.0490-24.2024. URL <https://www.jneurosci.org/content/early/2024/11/25/JNEUROSCI.0490-24.2024>. Publisher: Society for Neuroscience Section: Research Articles.
- Huang, Z., Wang, R., Shan, S., Li, X., and Chen, X. Log-Euclidean Metric Learning on Symmetric Positive Definite Manifold with Application to Image Set Classification. In *Proceedings of the 32nd International Conference on Machine Learning*, pp. 720–729. PMLR, June 2015. URL <https://proceedings.mlr.press/v37/huanga15.html>. ISSN: 1938-7228.
- Jaini, P. and Burge, J. Linking normative models of natural tasks to descriptive models of neural response. *Journal of Vision*, 17(12):16, October 2017. ISSN 1534-7362. doi: 10.1167/17.12.16. URL <https://doi.org/10.1167/17.12.16>.
- Karampatziakis, N. and Mineiro, P. Discriminative Features via Generalized Eigenvectors. *International conference on machine learning*, 2014.
- Kohn, A., Coen-Cagli, R., Kanitscheider, I., and Pouget, A. Correlations and Neuronal Population Information. *Annual Review of Neuroscience*, 39(1):237–256, 2016. doi: 10.1146/annurev-neuro-070815-013851. URL <https://doi.org/10.1146/annurev-neuro-070815-013851>. eprint: <https://doi.org/10.1146/annurev-neuro-070815-013851>.
- LeCun, Y., Bengio, Y., and Hinton, G. Deep learning. *Nature*, 521(7553):436–444, May 2015. ISSN 1476-4687. doi: 10.1038/nature14539. URL <https://www.nature.com/articles/nature14539>. Publisher: Nature Publishing Group.
- Ledoit, O. and Wolf, M. The Power of (Non-)Linear Shrinking: A Review and Guide to Covariance Matrix Estimation. *Journal of Financial Econometrics*, 20(1):187–218, January 2022. ISSN 1479-8409. doi: 10.1093/jfinec/nbaa007. URL <https://doi.org/10.1093/jfinec/nbaa007>.
- Lotte, F., Bougrain, L., Cichocki, A., Clerc, M., Congedo, M., Rakotomamonjy, A., and Yger, F. A review of classification algorithms for EEG-based brain–computer interfaces: a 10 year update. *Journal of Neural Engineering*, 15(3):031005, April 2018. ISSN 1741-2552. doi: 10.1088/1741-2552/aab2f2. URL <https://dx.doi.org/10.1088/1741-2552/aab2f2>. Publisher: IOP Publishing.
- Ly, A., Marsman, M., Verhagen, J., Grasman, R. P. P. P., and Wagenmakers, E.-J. A Tutorial on Fisher information. *Journal of Mathematical Psychology*, 80:40–55, October 2017. ISSN 0022-2496. doi: 10.1016/j.jmp.2017.05.006. URL <https://www.sciencedirect.com/science/article/pii/S0022249617301396>.
- Maheswaranathan, N., McIntosh, L. T., Tanaka, H., Grant, S., Kastner, D. B., Melander, J. B., Nayebi, A., Brezovec, L. E., Wang, J. H., Ganguli, S., and Baccus, S. A. Interpreting the retinal neural code for natural scenes: From computations to neurons. *Neuron*, 111(17):2742–2755.e4, September 2023. ISSN 08966273. doi: 10.1016/j.neuron.2023.06.007. URL <https://linkinghub.elsevier.com/retrieve/pii/S0896627323004671>.
- Mika, S., Ratsch, G., Weston, J., Scholkopf, B., and Mullers, K. Fisher discriminant analysis with kernels. In *Neural Networks for Signal Processing IX: Proceedings of the 1999 IEEE Signal Processing Society Workshop (Cat. No.98TH8468)*, pp. 41–48, August 1999. doi: 10.1109/NNSP.1999.788121. URL <https://ieeexplore.ieee.org/abstract/document/788121>.
- Miyamoto, H. K., Meneghetti, F. C. C., and Costa, S. I. R. The Fisher–Rao loss for learning under label noise. *Information Geometry*, 6(1):107–126, June 2023. ISSN 2511-249X. doi: 10.1007/s41884-022-00076-8. URL <https://doi.org/10.1007/s41884-022-00076-8>.
- Miyamoto, H. K., Meneghetti, F. C. C., Pinele, J., and Costa, S. I. R. On closed-form expressions for the Fisher–Rao distance. *Information Geometry*, 7(2):311–354, November 2024. ISSN 2511-249X. doi: 10.1007/s41884-024-00143-2. URL <https://doi.org/10.1007/s41884-024-00143-2>.
- Montesuma, E. F., Mboula, F. M. N., and Souloumiac, A. Recent Advances in Optimal Transport for Machine Learning. *IEEE Transactions on Pattern Analysis and Machine Intelligence*, 47(2):1161–1180, February 2025. ISSN 1939-3539. doi: 10.1109/TPAMI.2024.3489030. URL <https://ieeexplore.ieee.org/document/10740308/?arnumber=10740308>. Conference Name: IEEE Transactions on Pattern Analysis and Machine Intelligence.
- Moreno-Bote, R., Beck, J., Kanitscheider, I., Pitkow, X., Latham, P., and Pouget, A. Information-limiting

- correlations. *Nature Neuroscience*, 17(10):1410–1417, October 2014. ISSN 1546-1726. doi: 10.1038/nn.3807. URL <https://www.nature.com/articles/nn.3807>. Number: 10 Publisher: Nature Publishing Group.
- Movshon, J. A., Thompson, I. D., and Tolhurst, D. J. Spatial and temporal contrast sensitivity of neurones in areas 17 and 18 of the cat’s visual cortex. *The Journal of Physiology*, 283(1):101–120, 1978. ISSN 1469-7793. doi: 10.1113/jphysiol.1978.sp012490. URL <https://onlinelibrary.wiley.com/doi/abs/10.1113/jphysiol.1978.sp012490>. eprint: <https://onlinelibrary.wiley.com/doi/pdf/10.1113/jphysiol.1978.sp012490>.
- Nejatbakhsh, A., Garon, I., and Williams, A. Estimating Noise Correlations Across Continuous Conditions With Wishart Processes. *Advances in Neural Information Processing Systems*, 36:54032–54045, December 2023. URL https://proceedings.neurips.cc/paper_files/paper/2023/hash/a935ba2236c6ba0fb620f23354e789ff-Abstract-Conferece.html.
- Ni, L. and Burge, J. Feature-specific divisive normalization improves natural image encoding for depth perception, September 2024. URL <http://biorxiv.org/lookup/doi/10.1101/2024.09.05.611536>.
- Nielsen, F. A Simple Approximation Method for the Fisher–Rao Distance between Multivariate Normal Distributions. *Entropy*, 25(4):654, April 2023. ISSN 1099-4300. doi: 10.3390/e25040654. URL <https://www.mdpi.com/1099-4300/25/4/654>. Number: 4 Publisher: Multidisciplinary Digital Publishing Institute.
- Pedregosa, F., Varoquaux, G., Gramfort, A., Michel, V., Thirion, B., Grisel, O., Blondel, M., Prettenhofer, P., Weiss, R., Dubourg, V., Vanderplas, J., Passos, A., and Cournapeau, D. Scikit-learn: Machine Learning in Python. *Journal of Machine Learning Research*, 12:2825–2830, 2011.
- Pinele, J., Strapasson, J. E., and Costa, S. I. R. The Fisher–Rao Distance between Multivariate Normal Distributions: Special Cases, Bounds and Applications. *Entropy*, 22(4):404, April 2020. ISSN 1099-4300. doi: 10.3390/e22040404. URL <https://www.mdpi.com/1099-4300/22/4/404>. Number: 4 Publisher: Multidisciplinary Digital Publishing Institute.
- Rust, N. C., Schwartz, O., Movshon, J. A., and Simoncelli, E. P. Spatiotemporal Elements of Macaque V1 Receptive Fields. *Neuron*, 46(6):945–956, June 2005. ISSN 0896-6273. doi: 10.1016/j.neuron.2005.05.021. URL <https://www.sciencedirect.com/science/article/pii/S089662730500468X>.
- Sainburg, T., McInnes, L., and Gentner, T. Q. Parametric UMAP Embeddings for Representation and Semisupervised Learning. *Neural Computation*, pp. 1–27, August 2021. ISSN 0899-7667, 1530-888X. doi: 10.1162/neco_a.01434. URL https://direct.mit.edu/neco/article/doi/10.1162/neco_a_01434/107068/Parametric-UMAP-Embeddings-for-Representation-and
- Thanwerdas, Y. and Pennec, X. O(n)-invariant Riemannian metrics on SPD matrices. *Linear Algebra and its Applications*, 661:163–201, March 2023. ISSN 0024-3795. doi: 10.1016/j.laa.2022.12.009. URL <https://www.sciencedirect.com/science/article/pii/S0024379522004360>.
- Vazelhes, W. d., Carey, C. J., Tang, Y., Vauquier, N., and Bellet, A. metric-learn: Metric Learning Algorithms in Python. *Journal of Machine Learning Research*, 21(138):1–6, 2020. ISSN 1533-7928. URL <http://jmlr.org/papers/v21/19-678.html>.
- Weinberger, K. Q. and Saul, L. K. Distance Metric Learning for Large Margin Nearest Neighbor Classification. *Journal of Machine Learning Research*, 10:207–244, 2009.

A. Choice of Riemannian distance

Choosing an appropriate Riemannian distance in $\text{SPD}(m)$ is crucial for the performance of SQFA. First, we present in more detail the relationship between the affine-invariant distance and quadratic discriminability. Then, we show that other distances do not perform as well in practice.

A.1. Generalized eigenvalues reflect quadratic differences

The generalized eigenvalues λ_k and generalized eigenvectors \mathbf{v}_k of the pair of matrices $\mathbf{A} \in \mathbb{R}^{m \times m}$ and $\mathbf{B} \in \mathbb{R}^{m \times m}$ are the solutions to the generalized eigenvalue problem $\mathbf{A}\mathbf{v}_k = \lambda_k\mathbf{B}\mathbf{v}_k$. If \mathbf{B} is SPD, the solution to the problem is given by the eigenvalues of the matrix $\mathbf{B}^{-1/2}\mathbf{A}\mathbf{B}^{-1/2}$, where $\mathbf{B}^{-1/2}$ is the matrix inverse square root of \mathbf{B} . If \mathbf{A} and \mathbf{B} are identical, $\mathbf{B}^{-1/2}\mathbf{A}\mathbf{B}^{-1/2}$ is the identity matrix and all the eigenvalues are 1. The farther the generalized eigenvalues are from 1, the more different the matrices \mathbf{A} and \mathbf{B} are (i.e. the more different $\mathbf{B}^{-1/2}\mathbf{A}\mathbf{B}^{-1/2}$ is from the identity matrix).

Consider a random variable $\mathbf{z} \in \mathbb{R}^m$ that belongs to one of two classes i, j , with second moment matrices $\Psi_i = \mathbb{E}[\mathbf{z}\mathbf{z}^T | y = i]$ and $\Psi_j = \mathbb{E}[\mathbf{z}\mathbf{z}^T | y = j]$. Next, consider a vector $\mathbf{w} \in \mathbb{R}^m$ and the squared projection of \mathbf{z} onto \mathbf{w} , $(\mathbf{w}^T\mathbf{z})^2$. The following ratio relates to how different the squared projections are for the two classes, which is a useful proxy for quadratic discriminability:

$$R(\mathbf{w}) = \frac{\mathbb{E}[(\mathbf{w}^T\mathbf{z})^2 | y = i]}{\mathbb{E}[(\mathbf{w}^T\mathbf{z})^2 | y = j]} = \frac{\mathbf{w}^T\Psi_i\mathbf{w}}{\mathbf{w}^T\Psi_j\mathbf{w}} \quad (8)$$

where the second equality is obtained by taking the filter vector \mathbf{w} out of the expectation. The local extrema of the ratio $R(\mathbf{w})$ are obtained at the generalized eigenvectors $\mathbf{w} = \mathbf{v}_k$ of (Ψ_i, Ψ_j) , where the ratio $R(\mathbf{v}_k)$ equals the generalized eigenvalue λ_k . The ratio given by the right-hand side of Equation (8) is known as the generalized Rayleigh quotient. The more different λ_k is from 1, the more discriminable the classes i, j will be from the squared projection $(\mathbf{v}_k^T\mathbf{z})^2$. Also, it has been shown empirically that using as features the generalized eigenvectors \mathbf{v}_k with the eigenvalues λ_k most different from 1 leads to good quadratic discriminability between pairs of classes (Karampatziakis & Mineiro, 2014).

A.2. Affine-invariant metric is equivalent to Fisher information

For the reader unfamiliar with Riemannian geometry, it is useful to understand how a distance in a manifold is induced by a metric. (For an accessible introduction to Riemannian geometry see (Guigui et al., 2023).) Consider the curve $\gamma : [0, 1] \rightarrow \text{SPD}(m)$. Let $\gamma'(t)$ be the velocity vector of the curve at point $\gamma(t)$, which is a vector tangent to the curve. (The space of vectors tangent to a point in $\text{SPD}(m)$ is the space of symmetric matrices.) Like in Euclidean space, the length of the curve, $L(\gamma)$, is obtained by integrating the norm of the velocity (the speed) along the curve, i.e $L(\gamma) = \int_0^1 \|\gamma'(t)\|_{\gamma(t)} dt$. The geodesic between two points Ψ_i and Ψ_j in the manifold can be defined as the curve with the shortest length connecting them. The distance between Ψ_i and Ψ_j is the length of the geodesic connecting them.

The Riemannian metric is essential to define the norm of the tangent vector above. Like in Euclidean space, the norm of the tangent vector is given by the formula $\|\gamma'(t)\|_{\gamma(t)} = \sqrt{\langle \gamma'(t), \gamma'(t) \rangle_{\gamma(t)}}$. However, as indicated by the subscript, the inner product $\langle \cdot, \cdot \rangle_{\gamma(t)}$ depends on the base point $\gamma(t)$ at which it is being computed. The Riemannian metric determines at each point how the inner product is computed. Since the Riemannian metric determines the inner product, it is essential to determining the speed of the the curve at each point, and thus the distances in the manifold.

The affine-invariant distance emerges from using the affine-invariant metric to measure inner products. Consider the geodesic $\Psi : [0, 1] \rightarrow \text{SPD}(m)$ connecting Ψ_i and Ψ_j under the affine-invariant metric, where $\Psi(t)$ is the point in the geodesic at time t , $\Psi(0) = \Psi_i$, $\Psi(1) = \Psi_j$, and $\Psi'(t)$ is the velocity vector of the geodesic at point $\Psi(t)$. Under the affine-invariant metric, the squared norm of $\Psi'(t)$ is

$$\|\Psi'(t)\|_{\Psi(t)}^2 = \text{Tr}(\Psi(t)^{-1} \Psi'(t) \Psi(t)^{-1} \Psi'(t)) \quad (9)$$

This expression is equivalent (up to a factor of 2) to the Fisher information of the zero-mean Gaussian $\mathcal{N}(0, \Psi(t))$ in the direction $\Psi'(t)$, which can be denoted $\mathcal{I}(t)$ (see the explanation of Fisher information in Section 2.3.2). In mathematical terms, $\|\Psi'(t)\|_{\Psi(t)}^2 = 2\mathcal{I}(t)$. Fisher information sets a lower bound on how discriminable neighboring distributions are (see Section 2.3.2). Specifically, $\sqrt{\mathcal{I}(t)}$ is a measure of how discriminable $\mathcal{N}(0, \Sigma(t))$ and $\mathcal{N}(0, \Sigma(t + dt))$ are from observing samples of the distribution.

Using the definition of the distance as the integral of the speed along the geodesic, we have

$$d_{AI}(\Psi_i, \Psi_j) = \int_0^1 \sqrt{2\mathcal{I}(t)} dt \quad (10)$$

Thus the affine-invariant distance is the accumulated local discriminability (given by $\sqrt{\mathcal{I}(t)}$) of the infinitesimal perturbations that transform $\mathcal{N}(0, \Psi_i)$ into $\mathcal{N}(0, \Psi_j)$. This again suggests that d_{AI} is a good proxy for quadratic discriminability in the space of second-moment matrices.

The geometry of spaces of probability distributions with the Fisher information metric is known as information geometry, and the induced distances are known as Fisher-Rao distances. Thus, the affine-invariant distance in $\text{SPD}(m)$ is equivalent to the Fisher-Rao distance in the space of zero-mean Gaussians (Atkinson & Mitchell, 1981; Thanwerdas & Pennec, 2023). More broadly, the Fisher information can be used as a metric in other spaces of probability distributions, such as the space of Gaussians (Amari, 2016; Nielsen, 2023; Miyamoto et al., 2024), by taking the squared norm of a velocity vector in this space to be the Fisher information of the distribution in the direction of the velocity vector.

A.3. Comparison of distances

A.3.1. OTHER DISTANCES IN $\text{SPD}(m)$

To obtain empirical support for using the affine-invariant distance as a proxy for quadratic discriminability, we examined the performance of smSQFA when it uses for its objective function other distances in $\text{SPD}(m)$ (see (Congedo & Jain, 2019) for a review of different distances in $\text{SPD}(m)$). We used the smSQFA model because there are a large number of Riemannian distances with closed-form expressions in $\text{SPD}(m)$, some of them with information geometric interpretations. Specifically, we compared d_{AI} to four other distances: the Bures-Wasserstein distance, the Log-Euclidean distance, the Euclidean distance and the symmetric Kullback-Leibler (KL) divergence, or Jeffrey divergence.

The Bures-Wasserstein distance is given by

$$d_{BW}(\Psi_i, \Psi_j) = \sqrt{\text{Tr}(\Psi_i) + \text{Tr}(\Psi_j) - 2\text{Tr}\left(\left[\Psi_i^{1/2}\Psi_j\Psi_i^{1/2}\right]^{1/2}\right)} \quad (11)$$

The Bures-Wasserstein distance in $\text{SPD}(m)$ is equivalent to the optimal transport distance between zero-mean Gaussians (Thanwerdas & Pennec, 2023). The earth-mover's intuition of the optimal transport distance is that it measures how much work it takes to move a pile of dirt shaped like $\mathcal{N}(0, \Psi_i)$ to a pile of dirt shaped like $\mathcal{N}(0, \Psi_j)$.

The Log-Euclidean distance is given by

$$d_{LE}(\Psi_i, \Psi_j) = \|\log(\Psi_i) - \log(\Psi_j)\|_F \quad (12)$$

This distance is popular because it is a simple and computationally efficient way to measure distances in $\text{SPD}(m)$ (Huang et al., 2015). The Log-Euclidean distance is also a good approximation to the affine-invariant distance when the matrices are close to the identity matrix (Arsigny et al., 2006; Huang et al., 2015; Congedo & Jain, 2019).

The Euclidean distance is given by

$$d_E(\Psi_i, \Psi_j) = \|\Psi_i - \Psi_j\|_F \quad (13)$$

The Euclidean distance is rarely used in practice for SPD matrices because it does not take into account the geometry of $\text{SPD}(m)$.

The symmetric KL divergence between zero-mean Gaussians is given by

$$d_{KL}(\Psi_i, \Psi_j) = \frac{1}{2} (\text{KL}(\Psi_i, \Psi_j) + \text{KL}(\Psi_j, \Psi_i)) \quad (14)$$

where $\text{KL}(\Psi_i, \Psi_j) = \frac{1}{2} \left(\text{Tr}(\Psi_j^{-1}\Psi_i) + \log \frac{\det(\Psi_j)}{\det(\Psi_i)} \right) - m$ is the KL divergence between the zero-mean Gaussians $\mathcal{N}(0, \Psi_i)$ and $\mathcal{N}(0, \Psi_j)$. The KL divergence between two distributions is a measure of how different the two distributions are, and it is commonly used in statistics and machine learning. However, the KL divergence is not symmetric. The symmetric KL divergence is a symmetric version of the KL divergence, although it is not a true distance because it does not satisfy the triangle inequality.

A.3.2. COMPARISON OF DISTANCES IN TOY PROBLEM

To compare the distances, we designed a toy problem with 3 classes in 4 dimensions (Figure 7). The classes have zero mean and different covariance matrices. The covariance matrices are obtained by taking one covariance matrix and rotating it by different angles. Dimensions 1-2 have smaller (generalized) variance, but larger rotation between classes, making them more discriminative. Dimensions 3-4 have larger variance but smaller rotation, making them less discriminative.

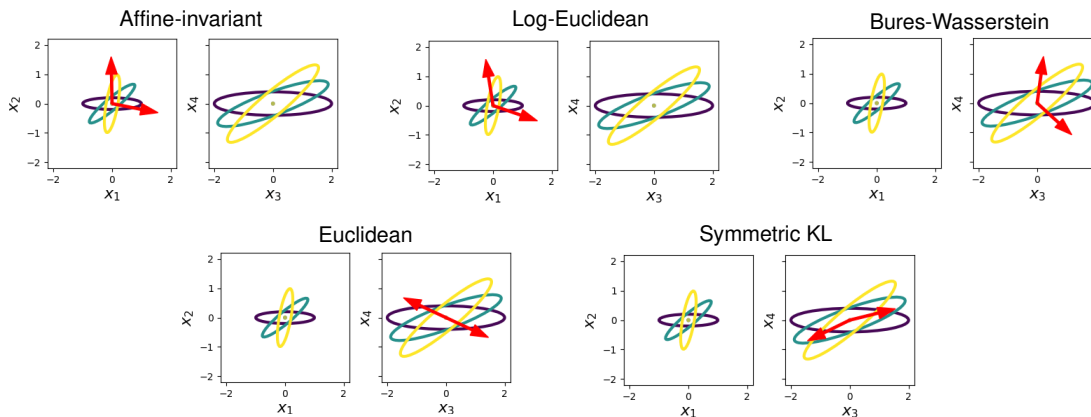


Figure 7. We learned 2 filters in the full 4 dimensional data space using different distances for the smSQFA objective. The ellipses show the distributions of the 3 classes, with the class indicated by color. The filters learned are shown as arrows overlaid on the data. The distance used to learn the filters is indicated in the title of each panel.

As expected, the filters learned using the affine-invariant distance are selective for dimensions 1-2, which are the most discriminative (Figure 7). On the other hand, the filters learned using the Bures-Wasserstein, Euclidean and symmetric KL divergence are selective for dimensions 3-4. For the Bures-Wasserstein distance, this can be explained using the earth-mover’s intuition: the effort to move the dirt piles increases with the scale of the Gaussians. Thus, for the goal of learning features that maximize second-order discriminability, the Bures-Wasserstein distance is not as useful as the affine-invariant distance.

Then, the filters learned using the Log-Euclidean distance are selective for dimensions 1-2. This is not surprising considering that the Log-Euclidean geometry is similar to the affine-invariant geometry (at least close to the identity matrix) (Huang et al., 2015; Arsigny et al., 2006). The Log-Euclidean distance might be a good choice for feature learning, with possible computational advantages over the affine-invariant distance.

A.3.3. COMPARISON OF DISTANCES IN REAL-WORLD DATASETS

We next tested the distances on the three datasets used in the main text. As expected, no distance performed better than the affine-invariant distance in any of the datasets (Figure 8). Notably, however, the Log-Euclidean distance performed as well as the affine-invariant distance for all datasets. This suggests that the Log-Euclidean distance might be a good alternative to the affine-invariant distance for feature learning. However, while the affine-invariant distance can be extended to take into account the means of the classes, like in smSQFA, there is no clear way to extend the Log-Euclidean distance to take into account the means.

These results show that choosing the right distance is crucial for the performance of SQFA. Furthermore, the affine-invariant distance performed better than alternatives commonly used in machine learning, like the Bures-Wasserstein (optimal transport) distance and the symmetric KL divergence. Because of the connection between the affine-invariant distance and the Fisher-Rao metric discussed in Appendix A.2, these results suggest that the Fisher-Rao metric more generally (i.e. not just in the space of zero-mean Gaussians) is a good proxy for discriminability.

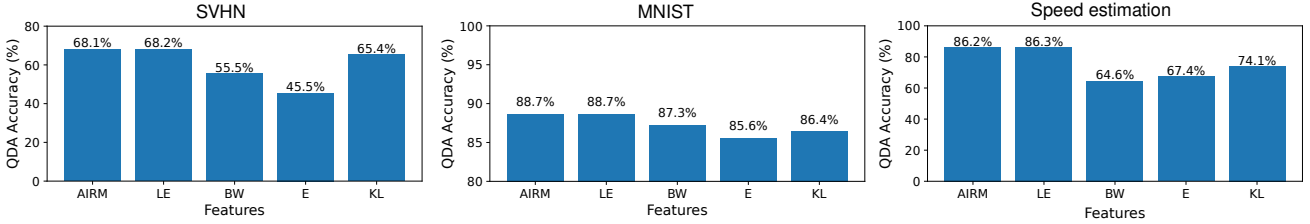


Figure 8. Accuracy of a QDA classifier using features learned by SQFA with different distances in $\text{SPD}(m)$. The same number of filters as in the main text were learned for each distance. **Left.** SVHN dataset. **Center.** Speed estimation dataset. **Right.** MNIST dataset. The distances are labeled as AIRM (affine-invariant), BW (Bures-Wasserstein), LE (Log-Euclidean), E (Euclidean) and KL (symmetric Kullback-Leibler).

B. Regularization and invariance

B.1. Invariance of affine-invariant distance

To better understand SQFA, it is important to consider the invariance properties of the affine-invariant distance. If $\mathbf{G} \in GL(m)$ where $GL(m)$ is the General Linear group, composed of non-singular m -by- m matrices, then a key property of the affine-invariant distance is that

$$d_{AI}(\Psi_i, \Psi_j) = d_{AI}(\mathbf{G}^T \Psi_i \mathbf{G}, \mathbf{G}^T \Psi_j \mathbf{G}) \quad (15)$$

(in words, the affine-invariant distance is invariant to the action by congruence of $GL(m)$). Note that if Ψ_i and Ψ_j are second-moment matrices of the variable \mathbf{z} for classes i, j respectively, then $\mathbf{G}^T \Psi_i \mathbf{G}$ and $\mathbf{G}^T \Psi_j \mathbf{G}$ are the second-moment matrices of the transformed variable $\mathbf{z}' = \mathbf{G}^T \mathbf{z}$ for these classes. This means that the affine-invariant distance is invariant to invertible linear transformations of the feature space. (If Ψ_i and Ψ_j are covariance rather than second-moment matrices, then d_{AI} is also invariant to translations in feature space.)

The invariance properties of d_{AI} have important implications for the features learned by SQFA. Specifically, let the filters $\mathbf{F} \in \mathbb{R}^{n \times m}$ be a maximum for Equation (1). Given the invariance described above, the filters $\mathbf{F}' = \mathbf{F}\mathbf{G}$ will also maximize the objective function. To see this, let Φ_i be the second moment matrix of the variable \mathbf{x} for class i . The second-moment matrix of $\mathbf{z} = \mathbf{F}^T \mathbf{x}$ is given by $\Psi_i = \mathbf{F}^T \Phi_i \mathbf{F}$. For the set of filters $\mathbf{F}' = \mathbf{F}\mathbf{G}$, then the second-moment matrix of $\mathbf{z}' = \mathbf{F}'^T \mathbf{x}$ satisfies

$$\Psi'_i = \mathbf{F}'^T \Phi_i \mathbf{F}' = \mathbf{G}^T \mathbf{F}^T \Phi_i \mathbf{F} \mathbf{G} = \mathbf{G}^T \Psi_i \mathbf{G} \quad (16)$$

Since all matrices Ψ'_i are related to the matrices Ψ_i by the same matrix \mathbf{G} , Equation (15) implies that the distances between the second-moment matrices are the same for \mathbf{F} and \mathbf{F}' .

This means that there is an equivalent set of solutions, given by the the sets of filters that span the same subspace (although see the next section). This can be a useful property, for example because there is no need to worry about scalings in the data space, since the scale of the filter outputs does not matter. But the lack of a unique solution also makes for less interpretable features (the interpretable object is the subspace spanned by the filters).

B.2. Regularization breaks invariance

The equivalence of solutions above, however, is eliminated when we introduce regularization as an additive term $\mathbf{I}\sigma^2$ to each second-moment matrix. Specifically, if we regularize the second-moment matrices by adding $\mathbf{I}\sigma^2$ to each matrix, such that $\Psi_i = \mathbf{F}^T \Phi_i \mathbf{F} + \mathbf{I}\sigma^2$, then it is no longer true that $\Psi'_i = \mathbf{G}^T \Psi_i \mathbf{G}$. Rather, there will be a different matrix \mathbf{G}_i satisfying $\Psi'_i = \mathbf{G}_i^T \Psi_i \mathbf{G}_i$ for each class i . Thus, Equation (15) no longer relates the distances for filters \mathbf{F} and $\mathbf{F}' = \mathbf{F}\mathbf{G}$, and the distances between second-moment matrices are no longer the same for both sets of filters.

One consequence of adding regularization is that the solution is no longer scale invariant. For filters with small norms, matrices $\Psi_i = \mathbf{F}^T \Phi_i \mathbf{F} + \mathbf{I}\sigma^2$ will be dominated by the regularization term, and thus more similar (i.e. closer) to each other. Then, the solution will tend towards filters with infinite norm that make the contribution of the regularization term negligible. In our case the filters (i.e. each column of \mathbf{F}) are constrained to have unit norm, so this is not a problem.

Following the same reasoning, the regularization term will penalize filters that lead to small second-moment matrices, since these will be dominated by the regularization term. Thus, regularization will favor the directions in the data space that lead to larger second-moment matrices. This might be useful in that it makes the filters more robust to estimation noise along dimensions with small variance, but it might also mask important information in directions with low squared values. Also, this makes the results dependent on the choice of the regularization parameter σ^2 . Future work will explore the effect of regularization on the features learned by SQFA, and examine how to choose the regularization parameter.

We note that regularization does not break the invariance of filter polarity, that is, the sign of the filters, and thus different runs of SQFA might lead to different signs of the filters.

C. LDA features maximize the Fisher-Rao distance between homoscedastic Gaussians

In this section, we prove Proposition 2.1.

For a labeled random variable $\mathbf{x} \in \mathbb{R}^n$ with class labels $y \in \{1, \dots, c\}$, the goal of drLDA can be described as finding the filters $\mathbf{F} \in \mathbb{R}^{n \times m}$ such that the variable $\mathbf{z} = \mathbf{F}^T \mathbf{x}$ maximizes the between-class scatter relative to the within-class scatter. Mathematically, this is typically formulated as maximizing the Fisher criterion, which is given by

$$\text{Tr}(\Sigma^{-1} \mathbf{S}_{\mathbf{z}}) \tag{17}$$

where Σ is the residual within-class covariance matrix of the data (i.e. the covariance matrix of the data after subtracting the class mean from each data point), and $\mathbf{S}_{\mathbf{z}}$ is the between-class scatter matrix of \mathbf{z} , defined as

$$\mathbf{S}_{\mathbf{z}} = \frac{1}{c} \sum_{i=1}^c (\mu_i - \mu)(\mu_i - \mu)^T$$

where μ_i is the mean of class i in the feature space and $\mu = \sum_{i=1}^c \mu_i$.

The cLDA classifier, which is typically paired with drLDA, is the optimal classifier assuming that the class-conditional distribution of \mathbf{z} is Gaussian, with different means μ_i for each class and a shared covariance matrix Σ . That is, the LDA classifier assumes $p(\mathbf{z}|y = i) = \mathcal{N}(\mu_i, \Sigma)$.

We wish to prove that the dimensionality reduction objective in Equation (17) is equivalent to maximizing the pairwise Fisher-Rao squared distances between classes under the distribution assumption of the LDA classifier. The Fisher-Rao distance between two Gaussians with shared covariance matrix Σ is given by (Pinele et al., 2020)

$$d_{\Sigma}(\mu_i, \mu_j) = \sqrt{(\mu_i - \mu_j)^T \Sigma^{-1} (\mu_i - \mu_j)} \tag{18}$$

The sum of pairwise squared Fisher-Rao distances between the classes is given by

$$\frac{1}{2} \sum_{i=1}^c \sum_{j=1}^c d_{\Sigma}(\mu_i, \mu_j)^2 = \frac{1}{2} \sum_{i=1}^c \sum_{j=1}^c (\mu_i - \mu_j)^T \Sigma^{-1} (\mu_i - \mu_j) \tag{19}$$

where the factor of 1/2 is included to control for double-counting. Thus, we must prove that the objectives in Equation (17) and Equation (19) are equivalent.

First, we assume without loss of generality that the overall mean $\mu = \sum_{i=1}^c \mu_i = 0$. (Note that both Equation (17) and

Equation (19) are invariant to translations in the feature space.) Then, we have

$$\begin{aligned}
 \frac{1}{2} \sum_{i=1}^c \sum_{j=1}^c d_{\Sigma}(\mu_i, \mu_j)^2 &= \frac{1}{2} \sum_{i=1}^c \sum_{j=1}^c (\mu_i - \mu_j)^T \Sigma^{-1} (\mu_i - \mu_j) \\
 &= \frac{1}{2} \sum_{i=1}^c \sum_{j=1}^c (\mu_i^T \Sigma^{-1} \mu_i + \mu_j^T \Sigma^{-1} \mu_j - 2\mu_i^T \Sigma^{-1} \mu_j) \\
 &= \sum_{i=1}^c \mu_i^T \Sigma^{-1} \mu_i - \sum_{i=1}^c \sum_{j=1}^c \mu_i^T \Sigma^{-1} \mu_j \\
 &= \sum_{i=1}^c \mu_i^T \Sigma^{-1} \mu_i - \left(\sum_{i=1}^c \mu_i^T \right) \Sigma^{-1} \left(\sum_{j=1}^c \mu_j \right) \\
 &= \sum_{i=1}^c \mu_i^T \Sigma^{-1} \mu_i \\
 &= \text{Tr} \left(\Sigma^{-1} \sum_{i=1}^c \mu_i \mu_i^T \right) \\
 &= c \text{Tr} (\Sigma^{-1} \mathbf{S}_{\mathbf{z}})
 \end{aligned}$$

In the first five lines we expanded the squared Fisher-Rao distance, used the linearity of the dot product and the fact that $\mu = 0$. In the last two lines we used the linearity and the cyclic property of the trace, and that $\sum_{i=1}^c \mu_i \mu_i^T = c \mathbf{S}_{\mathbf{z}}$ because $\mu = 0$. This shows that the objectives in Equation (17) and Equation (19) are equivalent.

D. Training times

For each dataset, we recorded the time it took to train the models on a consumer laptop with an 12th Gen Intel Core i7-1270P and 32 GB of RAM.

SQFA training times were in the order of seconds for all datasets (Figure 9). Remarkably, the training time for SQFA was comparable to that of LDA, ICA and FA, which are computationally efficient linear methods. It is worth noting that, while computing the affine-invariant distances involves computing the matrix inverse square root, which can be computationally expensive, this operation is only done for the second-moment matrices in the feature space in the case of smSQFA, and the embeddings in Equation (6) for SQFA. These are small matrices of size $m \times m$ for smSQFA and $m + 1 \times m + 1$ for SQFA. Thus, in cases where m is not large, the cost of each SQFA iteration is not high.

We note that SQFA training times were higher for the speed estimation dataset compared to the other datasets. This is partly because the filters were learned sequentially for this task, which is more computationally expensive than learning all filters at once.

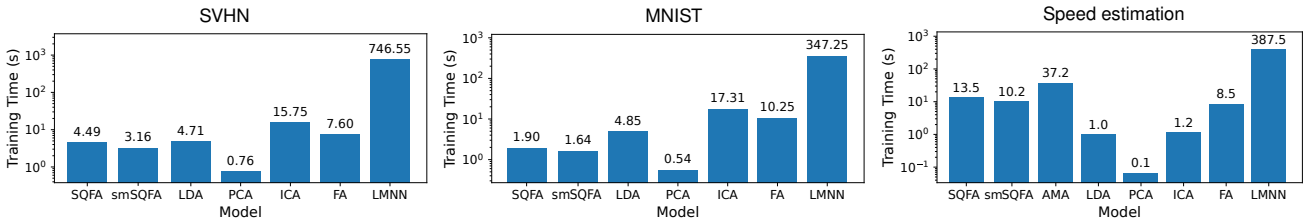


Figure 9. Training times for the different models on the different datasets. Times are in seconds, and indicated by the numbers on top of each bar. The y-axis is logarithmic. **Left:** SVHN. **Center:** MNIST. **Right:** Speed estimation dataset. We note that LMNN was trained on reduced datasets compared to the other methods (see Section 2.7). Also, LMNN training times were highly variable, unlike the other methods.

E. Details of the motion estimation task

E.1. Dataset synthesis

The motion estimation dataset consists of synthetic naturalistic videos of surfaces moving at different frontoparallel speeds, synthesized with the procedure described in (Burge & Geisler, 2015).

Briefly, each video is initially 60-by-60 pixels and 15 frames long. In this synthesis procedure, 60 pixels correspond to 1 degree of visual field (roughly equivalent to the foveal sampling of photoreceptors) and the videos have a duration of 250 ms (roughly equivalent to the duration of a fixation in natural viewing).

A video is synthesized by taking a random patch from an image of a natural scene and moving it horizontally at a given speed behind a 60-by-60 pixel aperture, for a duration of 15 frames. The resulting video is then filtered spatiotemporally to simulate the response of retinal photoreceptors to the video, as described in (Herrera-Esposito & Burge, 2024). Then, the resulting video is downsampled spatially by a factor of 2, to 30-by-30 pixel frames, and each frame is averaged vertically, leading to 30 pixel by 15 frame videos (thus, each video can be represented as a 450 dimensional vector). Vertically averaging the movies is equivalent to only considering filters that are vertically-oriented in the original 2D frame videos.

Then, to simulate further retinal processing, the video is converted to contrast, by subtracting and dividing by its mean intensity across pixels and frames. Denoting the resulting contrast video by \mathbf{c} , we apply divisive normalization to the video, dividing it by $\sqrt{(\|\mathbf{c}\|^2 + nc_{50}^2)}$ where $c_{50}^2 = 0.045$ is a constant and $n = 450$ is the number of pixels in the video multiplied by the number of frames. The resulting video simulates the retinal output in response to a naturalistic motion. See (Herrera-Esposito & Burge, 2024) and (Burge & Geisler, 2015) for more details and discussion on this synthesis procedure.

Above, we described the process by which a video is synthesized for a given speed. In the dataset, 41 retinal speeds (i.e. classes) were used, ranging from -6.0 to 6.0 deg/s with 0.3 deg/s intervals. For each of the 41 retinal speeds, we synthesized 800 different naturalistic videos, by using a different randomly sampled patch from a natural scene for each video. This adds nuisance naturalistic variability to the dataset. We used 500 videos per speed for training (a total of 20500 videos) and 300 videos per speed for testing (a total of 12300 videos).

Note that because the videos are generated with small patches randomly sampled from natural images, the expected intensity value at each pixel and frame is approximately the same (because natural image patches are approximately stationary), independent of speed. Then, because the videos were constrained to be contrast videos—i.e. they are formed by subtracting off and dividing by the intensity mean, consistent with early operations in the human visual system—the mean across patches equals zero, independent of speed. This results in a dataset where the classes are all approximately zero-mean.

E.2. AMA-Gauss training

Training of the AMA-Gauss model is described in (Jaini & Burge, 2017) and more recently in (Herrera-Esposito & Burge, 2024). Briefly, a set of linear filters is applied to each pre-processed video, and then a sample of independent noise is added to each filter output, obtaining the noisy response vector $\mathbf{R} = \mathbf{F}^T \mathbf{c} + \lambda$, where $\lambda \sim \mathcal{N}(0, \mathbf{I}\sigma^2)$. Then, a QDA-like classifier is used to classify the videos based on the noisy response vectors. The classifier assumes that the noisy response vectors are Gaussian distributed conditional on the speed (i.e. the class). To classify a video, the classifier computes the likelihood of the response given each class, that is, $p(\mathbf{R}|y = i)$. Then, using Bayes rule, the likelihoods and the priors (which are flat for the speed estimation dataset) are used to compute the posterior distribution $p(y|\mathbf{R})$. For a given video \mathbf{c} corresponding to true class $y = j$, the loss is the negative log-posterior at the correct class, that is, $-\log p(y = j|\mathbf{R})$. The filters \mathbf{F} that minimize the loss are obtained using gradient descent with the L-BFGS algorithm. The filters (columns of \mathbf{F}) are constrained to have unit norm. We use the same regularization parameter σ^2 for AMA-Gauss and for SQFA. Also like in SQFA, filters of AMA-Gauss are learned pairwise.